Journal of Alloys and Compounds 788 (2019) 1309–1321

Contents lists available at ScienceDirect

Journal of Alloys and Compounds

journal homepage: http://www.elsevier.com/locate/jalcom

Microstructure refinement and strengthening mechanisms of bimodal-sized and dual-phased (TiC_n-Al_3Ti_m)/Al hybrid composites assisted ultrasonic vibration

Qiang Li [a, b], Feng Qiu [a, b, d, *], Yu-Yang Gao [a, b], Bai-Xin Dong [a, b], Shi-Li Shu [a, b], Ming-Ming Lv [a, b], Hong-Yu Yang [a, c], Qing-Long Zhao [a, b], Qi-Chuan Jiang [a, b, **]

[a] State Key Laboratory of Automotive Simulation and Control, Jilin University, PR China
[b] Key Laboratory of Automobile Materials, Ministry of Education and Department of Materials Science and Engineering, Jilin University, Renmin Street NO. 5988, Changchun, Jilin Province, 130025, PR China
[c] School of Materials Science and Engineering, Jiangsu University of Science and Technology, Zhenjiang, 212003, Jiangsu, PR China
[d] Qingdao Automotive Research Institute of Jilin University, Qingdao, 266000, Shandong, PR China

ARTICLE INFO

Article history:
Received 21 December 2018
Received in revised form
26 February 2019
Accepted 27 February 2019
Available online 1 March 2019

Keywords:
In situ TiC_n-Al_3Ti_m particles
Hybrid composites
Grain refinement mechanisms
Strengthening mechanisms

ABSTRACT

Relatively high strength and good ductility are rarely obtained simultaneously in aluminum matrix composites. In the present work, dual-phased TiC_n-Al_3Ti_m (n: nanosized TiC particles and m: micron-sized Al_3Ti particles) particles were in situ synthesized in an Al-Ti-C system via the combustion synthesis method. Subsequently, (TiC_n-Al_3Ti_m)/Al hybrid composites were readily fabricated at high addition levels (0, 1, 3, 5 and 7 vol%) via the re-melting and diluting method assisted ultrasonic vibration. Then, the isolated influences of the dual-phased TiC_n-Al_3Ti_m particles on the solidification behaviors, microstructure evolution and mechanical properties, at both ambient- and elevated-temperatures, of aluminum alloys were systematically investigated. The experimental results revealed that the α-Al dendrites were substantially refined with a reduction of up to 4 times when compared with that of the unreinforced base alloy. Furthermore, at ambient temperature, 5 vol% (TiC_n-Al_3Ti_m)/Al exhibited the optimum comprehensive mechanical properties, and the yield and ultimate tensile strength were 124.3% and 165.2% higher than those of the unreinforced base alloy, whilst the fracture strain was not sacrificed. Theoretical calculations suggest that thermal-mismatch and Orowan strengthening effects contributed most to the yield strength increment, whereas the favourable fracture strain was achieved mainly due to grain refinement. Moreover, at elevated temperature (453 K), the yield strength and ultimate tensile strength were improved by 327.8% and 236.1%, respectively, whilst the fracture strain was still at a relatively high level of 29.2%. The improved thermal resistance primarily resulted from the pinning effects of the TiC_n-Al_3Ti_m particles on the grain boundaries and dislocations.

1. Introduction

Superior strength-ductility combination and thermodynamically stable aluminum alloys are urgently demanded for the aeronautical and automotive industries. Over decades, particle reinforced aluminum matrix composites (PRAMCs) have come to be preferred as the superb candidate for these industries due to their excellent synergistic attributes of rigid and thermostable particles and soft and light aluminum matrices [1–3]. However, the expectantly balanced strength-ductility is rarely obtained, especially at high addition levels, i.e., the strength-ductility trade-off dilemma [4]. Normally, the overall properties of PRAMCs are strongly dependent on the type and morphology, volume fraction, size distribution and spatial dispersion of the reinforcing particles as well as their interface bonding with the matrix [5,6].

Conventionally, extensive detailed investigations have been performed to study the strengthening and toughening potential of various particles on aluminum matrices, including SiC [7], TiB_2 [8], B_4C [9], Al_2O_3 [10], TiC [11], Al_3Ti [12,13], etc. and have achieved

* Corresponding author. State Key Laboratory of Automotive Simulation and Control, Jilin University, PR China.
** Corresponding author. State Key Laboratory of Automotive Simulation and Control, Jilin University, PR China.
E-mail addresses: qiufeng@jlu.edu.cn (F. Qiu), jqc@jlu.edu.cn (Q.-C. Jiang).

https://doi.org/10.1016/j.jallcom.2019.02.315
0925-8388/

great progress during the past decades. Thereinto, TiC has been extensively employed as a promising reinforcement to tailor the performance of aluminum alloys for its unique properties such as a high melting point, excellent thermal stability, high hardness and crystal structures similar to those of aluminum matrices [14–16]. Furthermore, Al_3Ti intermetallic particles have also been reported to possess good wettability, lattice matching with the aluminum matrix and better heterogeneous potency for aluminum alloys than do TiC, AlB_2 [17] and TiB_2 [17,18]. Additionally, the merits of micron-sized or nanosized particles have also been discussed and investigated [19].

Currently, bimodal-sized (micron-nano) particles are generally demonstrated to present more efficient refining and strengthening of the metal matrices over their single-sized counterparts. Tian et al. [20] reported that an Al-Cu composite reinforced by bimodal-sized TiC particles exhibited finer microstructure and higher room- and high-temperature strength and ductility when compared to those of the composites with only an individual nano- or micron-sized TiC addition. Similar results have also been revealed by other researchers in recent years [21,22]. Furthermore, innovative aluminum matrix hybrid composites have been developed recently and recognized as the new promising generation of composites for simultaneously possessing the attributes of more than one type of added particles. Resultantly, the composites usually exhibited better comprehensive performances than did the counterparts reinforced with mono-particles [23–26]. A recent study by Hu et al. [27] reported that the fabricated (B_4C-Al_3Ti)/Al hybrid composite possessed a higher hardness and tensile strength, but the ductility of the hybrid composite was lower than that of the Al matrix. It should be mentioned that previous research mainly concentrated on the hybrid composites reinforced by ex situ dual particles [28,29]. In contrast, compared with the performance of PRAMCs prepared via ex situ processing methods, the in situ PRAMCs usually exhibit better comprehensive mechanical properties due to their stronger interfacial bonding and better wettability between the particles and their matrix as well as more well-dispersed particles [30,31]. Conclusively, it will be a more effective strategy to achieve an excellent combination of strength and ductility by simultaneously incorporating in situ nanosized TiC and micron-sized Al_3Ti particles into the matrix. As per our knowledge, few studies have been dedicated to the fabrication of hybrid composites reinforced by dual-phased TiC-Al_3Ti particles with bimodal sizes at high addition levels and the study of the corresponding microstructure evolution and room- and elevated-temperature mechanical properties. Additionally, the solutes and precipitates in the aluminum alloys will inevitably interact with the added particles during solidification and the subsequent heat treatment [32,33], which will affect the study of the isolated influences of in situ dual-phased particles on the performances of the hybrid composites. However, few researchers have been conscious of this point in the past years.

In previous reports, in situ particles are commonly synthesized through the direct aluminum melt reaction method [34,35], whereas, it is well acknowledged that the incorporation of particles via master alloys could facilitate their homogeneous spatial dispersion in the molten aluminum. Furthermore, among those reported manufacturing methods for hybrid composites, powder metallurgy and melt processing are the most commonly used techniques [23]. However, the former is limited at the laboratory scale as several pores may be introduced into the composites, such that post-fabrication deformation processes are required to diminish the defects for improving the mechanical properties [29,36]. Comparatively, the latter exhibits great potential and is preferred as the most suitable approach for hybrid composites in terms of near-net shape, cost-effective and mass production. However, there are remaining issues and challenges: (1) The inherent agglomeration inclination of nanosized particles in molten aluminum. Unfortunately, the traditional mechanical stir method has been proven to be invalid or inefficient. (2) Weak interfacial bonding caused by interfacial reactions between the reinforcements and the melt, which directly restricts the load transfer efficiency. In this context, a novel manufacturing technique, the melt processing assisted by re-melting and diluting method under high-intensity ultrasonication, is proposed for the fabrication of (TiC_n-Al_3Ti_m)/Al hybrid composites in our work.

The present research attempts to synthesize an efficient in situ dual-phased TiC_n-Al_3Ti_m strengthening additive with favourable particle ratios and size distribution by combustion synthesis for aluminum and its alloys. Afterwards, the dual-phased TiC_n-Al_3Ti_m particles were incorporated into the pure Al at high addition levels. Then, the isolated role of the fabricated in situ dual-phased TiC_n-Al_3Ti_m particles on the solidification processing, microstructure evolution and mechanical properties of aluminum alloys were investigated. The underlying microstructure refinement mechanism, strengthening mechanisms at both ambient- and elevated-temperatures of the hybrid composites were discussed systematically. It is reasonable to assume that this work may provide a new perspective for the composition design and engineering applications of particle reinforced aluminum matrix composites.

2. Experimental procedure

Fig. 1 represents the processing schematic for in situ bimodal-sized and dual-phased (TiC_n-Al_3Ti_m)/Al hybrid composites. In this study, the processing procedure mainly included two parts: the preparation of Al-30 vol% (TiC_n-Al_3Ti_m) master alloys by combustion synthesis and the subsequent fabrication of (TiC_n-Al_3Ti_m)/Al hybrid composites by re-melting and diluting method assisted

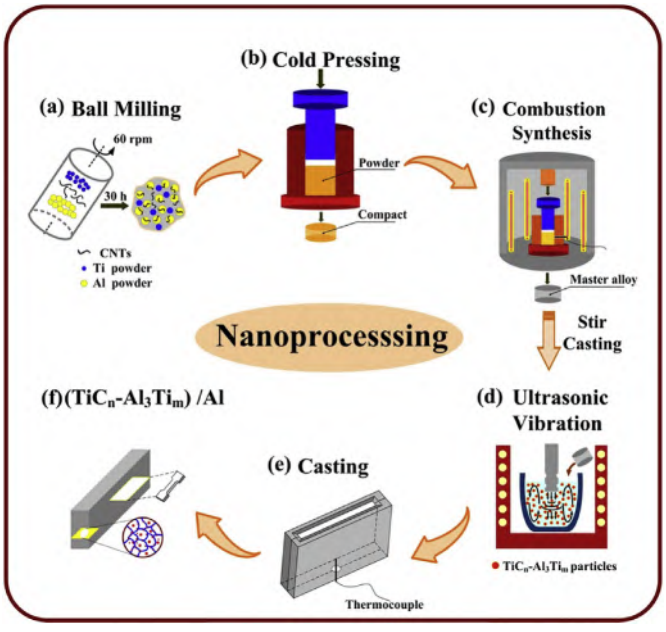

Fig. 1. The processing schematic for the in situ dual-phased (TiC_n-Al_3Ti_m)/Al hybrid composites: (a) mixing CNTs, Al and Ti powders adequately via ball milling, (b) pressing the blends into compacts, (c) the combustion synthesis and hot pressing of the compacts into master alloys, (d) introducing the TiC_n-Al_3Ti_m particles into the pure Al melt via the re-melting and diluting method and then dispersing the dual-phased particles uniformly by high-intensity ultrasonication, (e) casting the molten melt into a steel mould and monitoring the temperature variations with time and (f) sampling of the microstructures and tensile testing of the hybrid composites.

ultrasonic vibration.

2.1. Preparation of Al-30 vol% (TiC_n-Al_3Ti_m) master alloys

As illustrated in Fig. 1(a–c), the preparation process of Al-30 vol % (TiC_n-Al_3Ti_m) master alloys (wherein the volume ratio of Al, TiC and Al_3Ti was 70: 25: 5) could be divided into three steps: First, carbon nanotubes (CNTs) (99.5% purity, 10 nm–20 nm in diameter and 20 μm–100 μm in length), Ti (99.5% purity, ~25 μm) and Al powders (99.5% purity, ~48 μm) as reactants were ball milled sufficiently into a blend at 60 rpm for 30 h. The powder to ball ratio during the ball milling was 1:10. Subsequently, the fabricated blends were densified into compacts with dimensions of 30 mm in diameter and 40 mm in height. During the cold pressing, the pressure increased with time until 60 KN and dwelled for 15s. Finally, the combustion synthesis and hot pressing of the compacts was undertaken in a vacuum thermal explosion furnace at 1143 K. The high temperature for reactions was provided by the graphite electrode rods via radiation inside the vacuum furnace. While during the hot pressing, the pressure was around 40 MPa and was held for 5 min.

2.2. Fabrication of in situ dual-phased (TiC_n-Al_3Ti_m)/Al hybrid composites

The melt processing is illustrated in Fig. 1(d–f). According to the nominal addition amounts of 1, 3, 5 and 7 vol%, the dual-phased TiC_n-Al_3Ti_m particles were added into the commercial pure Al melt in the form of Al-30 vol% (TiC_n-Al_3Ti_m) master alloys and stirred by a graphite rod at 1073 K for 3 min, then, high-intensity ultrasonication with a niobium alloy probe was submerged into the melt to uniformly disperse the TiC and Al_3Ti particles for 5 min. Afterwards, the molten aluminum was degassed by hexachloroethane at 1023 K and stirred for 5 min, then the slag and oxide skin were skimmed off. After isothermally held for 3 min, the melt was finally poured into a preheated steel mould (up to 373 K) with dimensions of $200 \times 20 \times 150\ mm^3$. Simultaneously, as seen in Fig. 1(e), the temperature variations with time during solidification were monitored and recorded with a thermocouple inserted from the bottom of the mould. The melt temperature was recorded through a data logger with a frequency of 100 Hz and a precision of 0.1 °C. Nucleation arrests of the prepared alloys were identified in the first derivatives (dT/dt) of the obtained cooling curves according to the treatment employed in Ref. [37]. For convenience, the fabricated hybrid composites are hereafter named as HC-1, HC-3, HC-5 and HC-7. Additionally, a pure Al ingot, without TiC_n-Al_3Ti_m addition, was casted as the reference alloy with a similar process to the procedure above and is termed Pure Al.

2.3. Characterization

X-ray diffraction (XRD) was performed to determine the phase constitutions of the Al-30 vol% (TiC_n-Al_3Ti_m) master alloys and hybrid composites. The final content of each phase in the master alloy could be calculated by the formula below [38]:

$$W_i = \frac{I_i/RIR_i}{\sum_{i=1}^{N}(I_i/RIR_i)} (1 \le i \le N) \quad (1)$$

where W_i represents the weight fraction of the synthesized phase i in the master alloy. I_i represents the integrated intensity of the highest diffraction of each phase. N represents 3 in our work. RIR_i

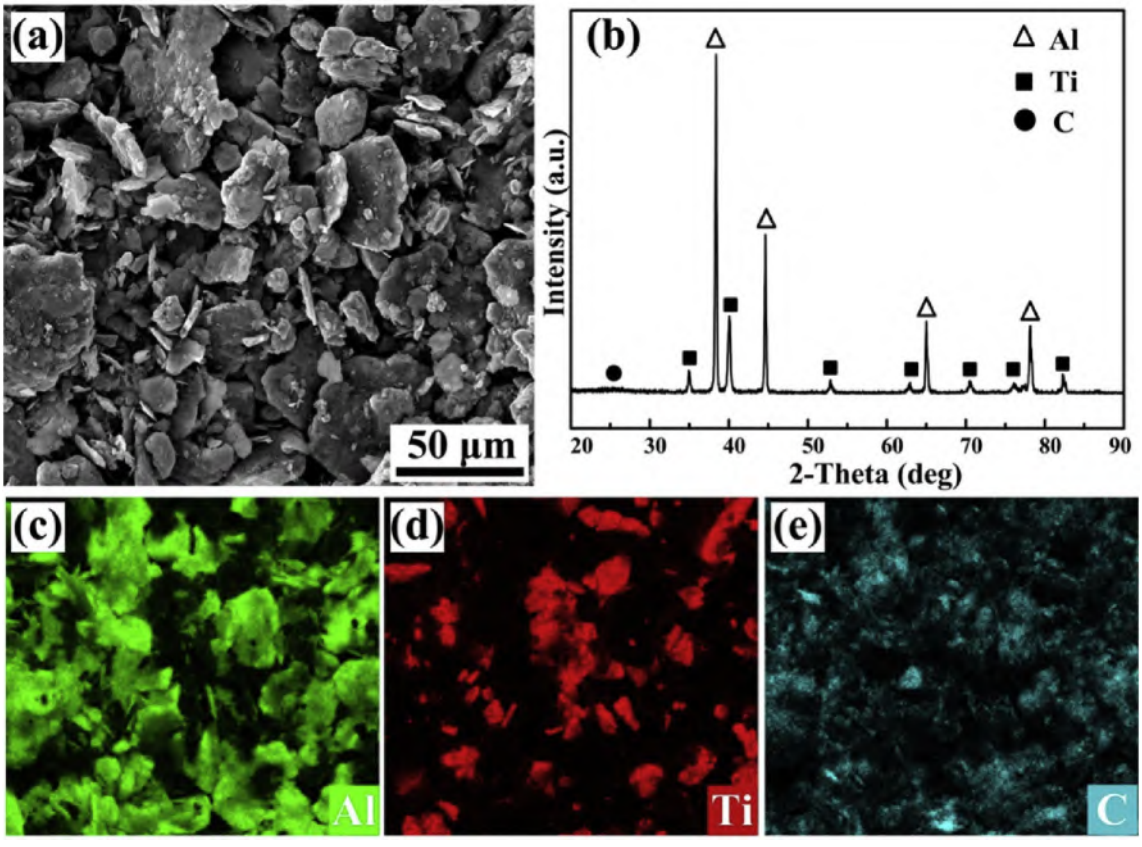

Fig. 2. (a) The SEM micrograph and (b) XRD spectrum of the ball milled blends; the EDS analysis of (c) Al, (d) Ti and (e) CNTs in the blends.

represents the value in the PDF cards.

The nanosized TiC particles were extracted by a 10 vol% hydrochloric acid solution, and afterwards, the size distribution and morphologies of the particles were analysed by a field emission scanning electron microscope (FESEM, JSM-6700F, Japan). To calculate the average diameters of the TiC and Al_3Ti particles in the master alloys, as least twenty SEM and FESEM micrographs were used to analyze the particle sizes and their distributions using the Nano Measurer software. The metallographic specimens were mechanically ground, polished and etched by Keller's reagent. Then, the specimens were characterized by an optical microscope (OM, Olympus PMG3, Japan), scanning electron microscopy (SEM, Tescan vega3 XM, Czech Republic) equipped with an energy dispersive spectrometer (EDS), and transmission electron microscopy (TEM, JEM-2100F, Japan). Tensile testing at 298 K and 453 K (MTS 810, USA) was carried out with the same dog-bone shaped specimens with a gauge cross-section of 4.0×2.5 mm^2 and a gauge length of 10.0 mm under a tensile rate of 1×10^{-4}.

3. Results and discussion

3.1. Microstructure analysis of the Al-(TiC_n-Al_3Ti_m) master alloy

Fig. 2(a) showed the SEM photograph of the ball milled Al powders, Ti powders and CNTs. It is clear that lots of small particles were embedded in or adhered to the surface of large particles. The XRD pattern of the milled powder blends was also characterized and showed in Fig. 2(b). As can be seen, only Al, Ti and C raw reactants can be detected, indicating that there was no reactivity among Al, Ti and C during the ball-milling step. Moreover, from the

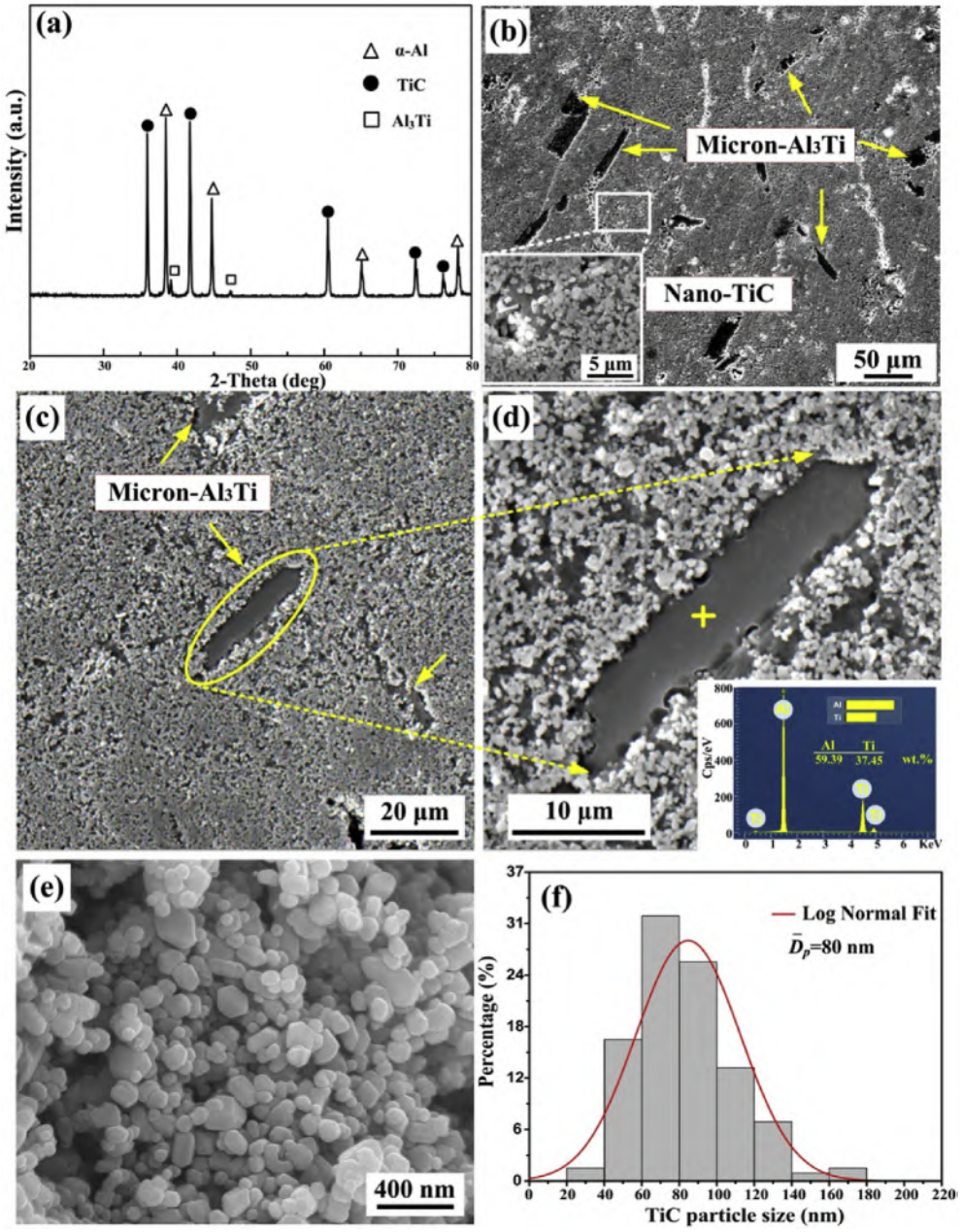

Fig. 3. (a) The XRD spectrum and SEM micrographs of (b) the Al-30 vol% (TiC_n-Al_3Ti_m) master alloy, (c) the Al_3Ti particles in the master alloy, (d) the magnification micrograph of a typical Al_3Ti particle. (e) A FESEM micrograph showing the morphology of the extracted TiC particles and (f) the corresponding statistical size distribution plot of the TiC particles.

EDS analysis in Fig. 2(c–e), the powders had been mixed uniformly.

As shown in Fig. 3(a), the diffraction peaks of TiC, Al_3Ti and α-Al phases were clearly detected in the master alloy. According to formula (1), the volume ratio of TiC, Al_3Ti and α-Al phases in Al-(TiC_n-Al_3Ti_m) master alloy could be determined as 24: 6: 70. As aforementioned, the size distribution and morphologies of reinforcing particles are critical to the resultant performance of hybrid composites. The corresponding microstructure of the as-prepared Al-(TiC_n-Al_3Ti_m) master alloy is shown in Fig. 3(b). As observed, several micron-sized Al_3Ti particles, identified by the EDS spectrum inserted in Fig. 3(d), were uniformly distributed throughout the microstructure. Otherwise, it is worth noting that the content of Al_3Ti particles was properly controlled in our work. The typical view of Al_3Ti particles, appearing with a block-like morphology with an average size of 30 μm, is further clearly shown in Fig. 3(c and d). Moreover, as shown in the magnification micrograph in Fig. 3 (b), it can be noticed that the nanosized TiC particles were spread out uniformly on the Al matrix. The three-dimensional morphology of nanosized TiC particles was further revealed by the FESEM micrograph in Fig. 3(e). As observed, the in situ formed TiC particles largely displayed a spheroidal shape, rendering them effective for load transfer and avoiding stress concentration as reinforcements in the interior of the matrix under external loading. According to the statistical result in Fig. 3(f), the TiC particles presented a narrow size distribution ranging from 40 to 120 nm, and the average size was 80 nm. In other words, nanosized TiC particles were successfully obtained.

3.2. *Microstructures of in situ dual-phased (TiC_n-Al_3Ti_m)/Al hybrid composites*

The grain refinement response of the commercial pure Al to the as-fabricated in situ dual-phased TiC_n-Al_3Ti_m particles at varying volume fractions is exhibited in Fig. 4(a–e). It can be easily found that the coarse and columnar dendrite structures in Pure Al gradually transformed into finer and equiaxed dendrites with increasing addition levels. Specifically, the average grain size variations as a function of TiC_n-Al_3Ti_m particles addition are illustrated in Fig. 5 to quantitatively assess the refining efficacy of the hybrid composites. As observed, the grain size decreased steeply from 270 μm to 99 μm upon addition of 1 vol% dual-phased TiC_n-Al_3Ti_m particles. Then, the grain refining efficiency gradually tended to saturate, and the grain sizes decreased marginally, in spite of the significantly increased particle addition. Ultimately, the hybrid composites reinforced by 7 vol% TiC_n-Al_3Ti_m particles exhibited the finest equiaxed structure with an average size of 70 μm, reduced by 74.1% compared with that of the unreinforced Pure Al. Additionally, compared with our previously reported nanosized SiC particles in pure Al [19], the in situ dual-phased TiC_n-Al_3Ti_m particles exhibited a more prominent grain refinement efficiency, as explicitly displayed in Fig. 5.

From the micrographs in Fig. 4(a–e), it could be observed that

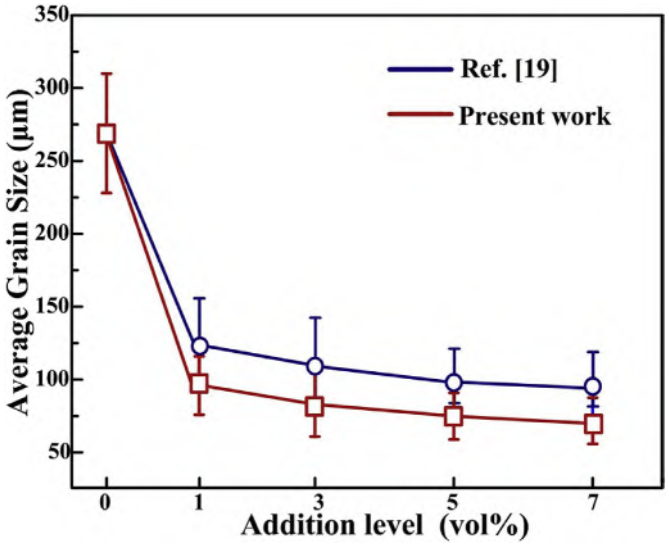

Fig. 5. The grain sizes of α-Al in the hybrid composites varying with the addition levels of in situ dual-phased TiC_n-Al_3Ti_m particles and a comparison against those in Ref. [19].

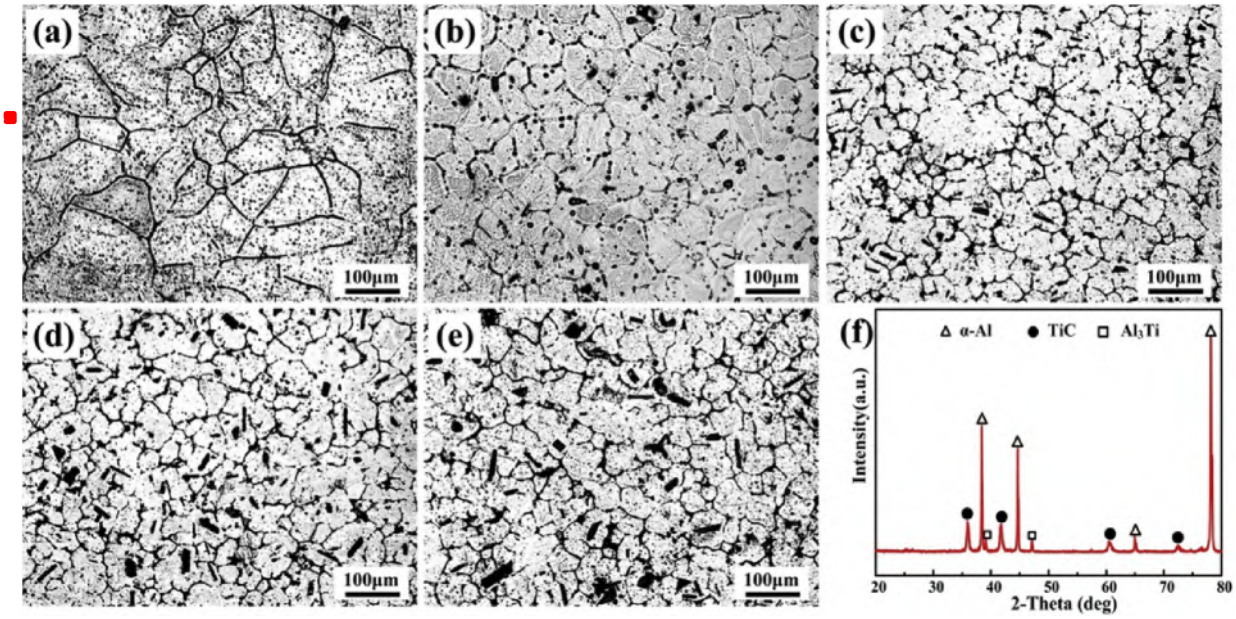

Fig. 4. Metallographic micrographs of the Pure Al and hybrid composites reinforced by different addition levels of in situ dual-phased TiC_n-Al_3Ti_m: (a) Pure Al, (b) HC-1, (c) HC-3, (d) HC-5, (e) HC-7. (f) The XRD spectrum of HC-7.

the in situ formed Al_3Ti particles, the black and block-like phases as confirmed by the XRD spectrum in Fig. 4(f), were well-distributed throughout the matrix and increased with the addition of dual-phased TiC_n-Al_3Ti_m particles. Moreover, the average size of Al_3Ti particles in Fig. 4(a–d) was refined to 10–20 μm after re-melting and diluting under ultrasonic vibration. Consequently, this Al_3Ti phase could serve as an effective and ideal reinforcement in terms of morphology and size [31]. However, when at the higher addition level of 7 vol%, it should be noted that the Al_3Ti particles became larger in size and were distributed at both transgranular and interdendritic regions, even across whole α-Al grains. Furthermore, the nanosized TiC particles in the hybrid composites were analysed in more detail by TEM. As seen in Fig. 6(a), a typical portion of nanosized particles with a spheroidal shape, verified as TiC by SAED in Fig. 6(b), was incorporated and dispersed homogeneously in the interior of the α-Al grain via the assisted acoustic streaming and cavitation nonlinear effects of ultrasonic vibration, which is particularly important as a prerequisite for excellent performance. Moreover, as revealed in Fig. 6(c), it is evident that the integrity interface between the nanosized TiC particle and matrix was clean and well-bonded, which indicated that no interface reaction or oxidation occurred during solidification. It is natural that this strong interfacial bonding will perform excellent load transfer capacity from the soft aluminum matrix to the rigid TiC particles.

To track the role of as-fabricated dual-phased particles during solidification, the solidification histories of the commercial pure Al prior to and after the introduction of 1 and 5 vol% in situ TiC_n-Al_3Ti_m particles were selected and monitored during cooling and are depicted by the cooling curves in Fig. 7. As shown in Fig. 7(a), the solidification path of pure Al was substantially altered. Moreover, as shown in Fig. 7(b–d), compared with that of Pure Al, the nucleation arrests of the other two hybrid composites were shifted continually towards higher temperatures with increasing addition levels. Specifically, the nucleation temperatures of Pure Al, HC-1 and HC-5 were 654.4 °C, 661.1 °C and 666.6 °C, respectively, which indicated that the in situ dual-phased TiC_n-Al_3Ti_m particles were potent to trigger the heterogeneous nucleation of α-Al crystals during cooling. Furthermore, a clear recalescence phenomenon was observed at 651.7 °C in the solidification process of Pure Al, while this characteristic event was greatly suppressed in the presence of TiC_n-Al_3Ti_m particles. Based on the classical nucleation model by M – H [39], the newly formed crystals will be stifled in advance upon the initiation of recalescence. Thus, the nucleation behaviour in the unreinforced Pure Al will stop in advance, which leads to the formation of more developed dendrites.

The synergistic effects of Al_3Ti and TiC particles on the solidification microstructures of the hybrid composites, i.e., nucleation and subsequent dendrite growth, are sketched in Fig. 8(a). It is reported that the wettability and crystallographic matching relationships between the inoculants and metal nuclei play a key role in determining the heterogeneous nucleation potency of the inoculants [40]. However, the wettability between ceramic particles and Al matrix is relatively poor [13]. Moreover, the orientation relationships between Al_3Ti or TiC particles and Al matrix and their comparison have been reported in Ref. [17]. According to the edge-to-edge matching model, Al_3Ti particles are more effective as heterogeneous substrates for α-Al crystal than TiC ceramic particles. Actually, particle sizes of Al_3Ti phase ranged from smaller than 10 μm [13,31] to 6–20 μm [41] all showed great grain refinement efficiency. So, in our work, it may be more likely that the micron-sized Al_3Ti particles provide nucleation sites for the α-Al. In this regard, the thermostable α-Al nuclei will be initiated and emerge preferentially on micron-sized Al_3Ti, instead of nanosized TiC particles, when the bulk liquid is thermally undercooled sufficiently to surmount the barrier for free growth. These similar nucleation events occur simultaneously and continue progressively in the whole melt until the appearance of recalescence, where the thermal undercooling is totally offset by the latent heat released by the growth of the newly formed nuclei. Afterwards, the final grain size will be under the control of grain growth of the dendrites. As clearly seen in Figs. 6(a) and 8(b), nanosized TiC particles were partially engulfed by the advancing solidification front and trapped in the solidified α-Al dendrites. Whereas the majority of TiC particles will be pushed and undergo self-assembly adsorbed around the growing α-Al, such that the diffusion of Al atoms in the remaining liquid onto the S/L interface required for the dendrite growth will be inhibited. As a result, the growth of dendrites will be restricted powerfully until their impingement and coalescence. It can be conferred that this inhibited growth effect will be more significant with an increase in TiC addition. Accordingly, finer and equiaxed α-Al dendrites with an even size distribution will form in the final solidification structure. Then, these pile-up nanosized TiC particles will dwell along the last solidifying regions, i.e., grain boundaries, and form quasi-network architecture [42], as shown in Fig. 8(c).

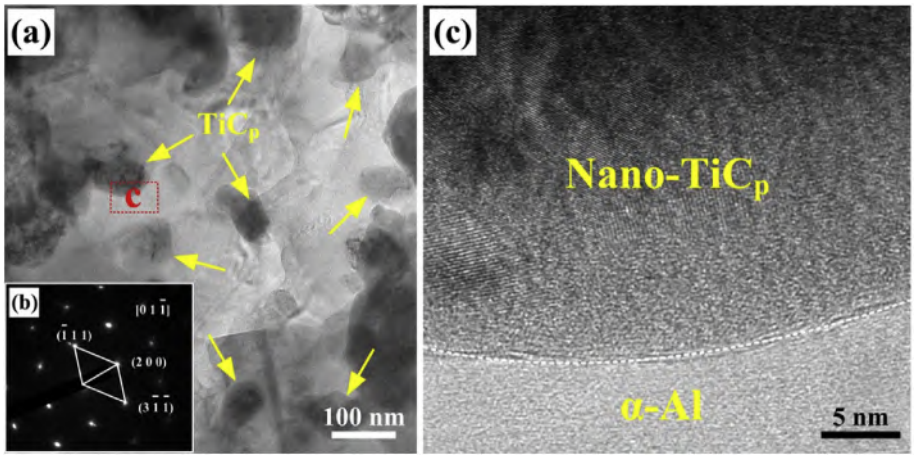

Fig. 6. TEM micrographs of the HC-5 hybrid composites: (a) the distribution of nanosized TiC particles (nano-TiC_p) in the hybrid composite, (b) the corresponding selected area electron diffraction (SAED) pattern of a TiC particle and (c) the high-resolution transmission electron microscopy (HRTEM) micrograph of the interface between a nanosized TiC particle and the matrix.

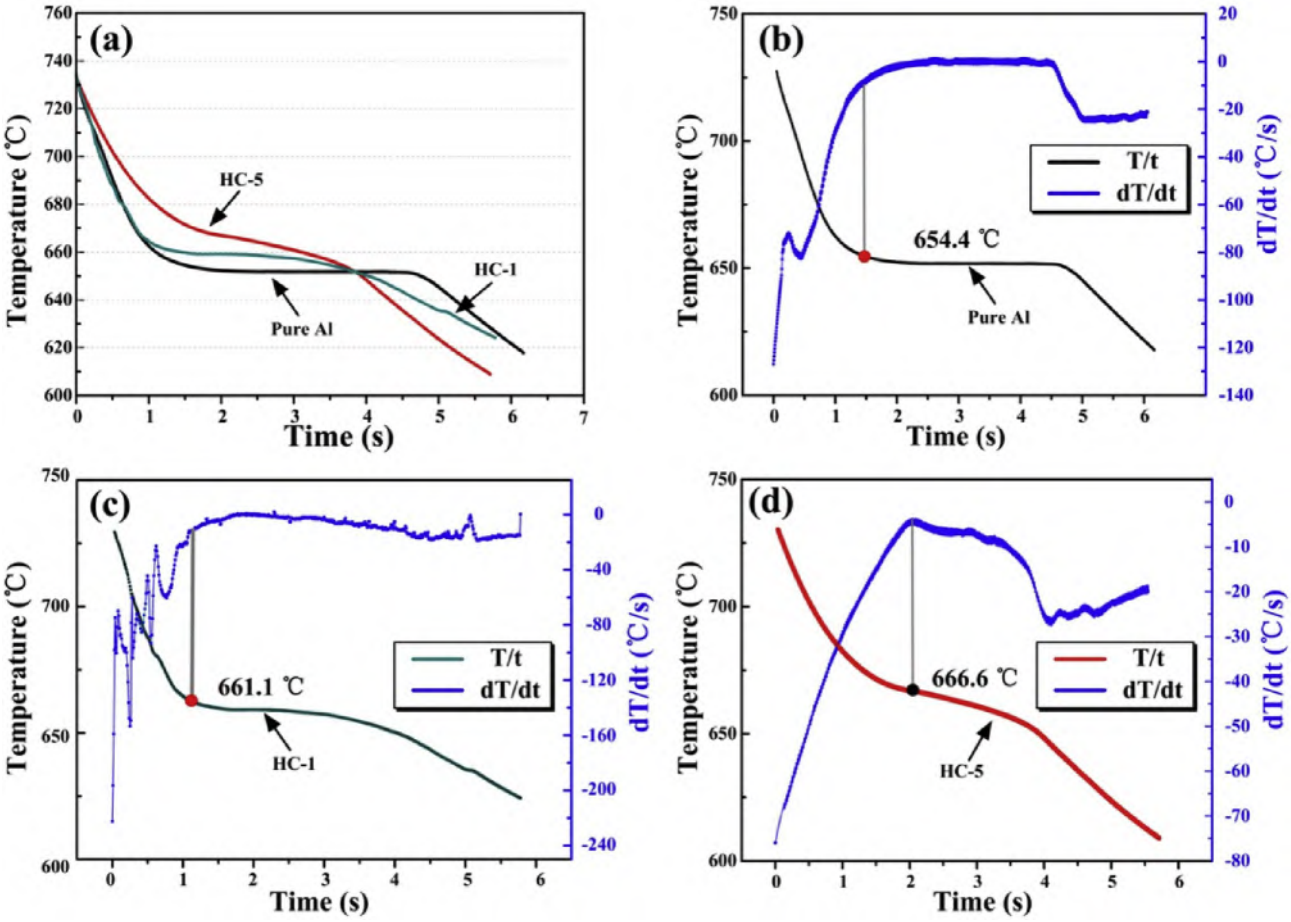

Fig. 7. (a) Cooling curves of the Pure Al and hybrid composites containing 1 and 5 vol% in situ dual-phased TiC_n-Al_3Ti_m particles and the corresponding cooling rate curves of (b) Pure Al, (c) HC-1 and (d) HC-5.

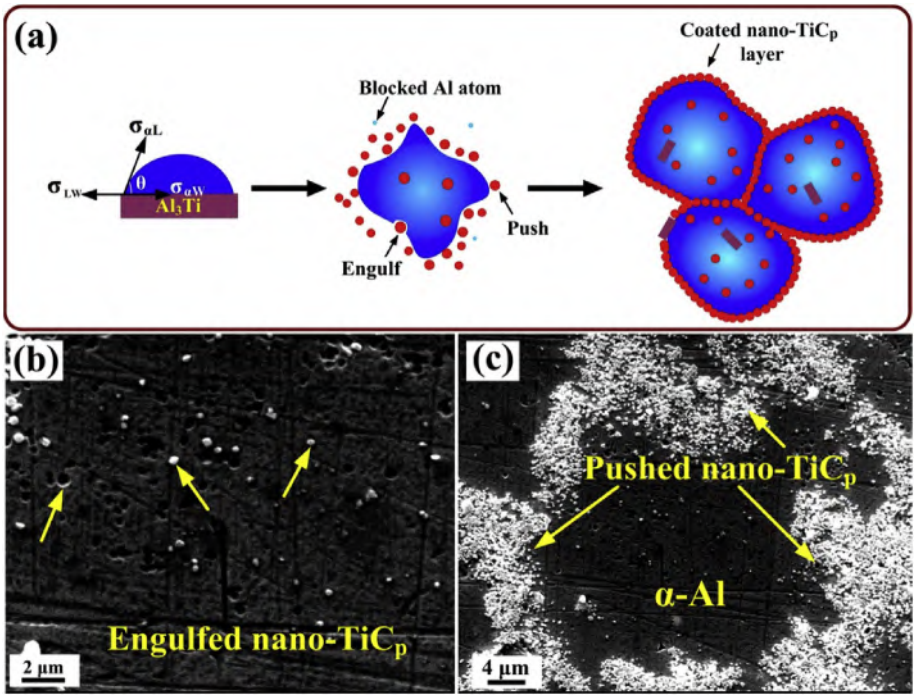

Fig. 8. (a) Schematic representation of the synthetic effects of Al_3Ti and TiC particles on the nucleation and growth process of α-Al dendrites in hybrid composites during solidification, (b) the particles engulfed within α-Al and (c) pushed nanosized TiC particles along grain boundary at the 5 vol% addition level.

3.3. Mechanical properties

3.3.1. Tensile properties at ambient temperature

Typical tensile curves at ambient temperature (298 K) of the Pure Al and the hybrid composites containing various amounts of TiC_n-Al_3Ti_m particles are presented in Fig. 9(a), along with the corresponding statistical data given in Fig. 9(b) and Table 1. As exhibited in Fig. 9(a), the fabricated alloys underwent near-yielding, uniform deformation, necking, nonuniform deformation and final rupture. It is clear in Fig. 9(b) that both the yield strength ($\sigma_{0.2}$) and ultimate tensile strength (σ_b) of the hybrid composites were pronouncedly enhanced in contrast with those of the unreinforced Pure Al, and these values increased continually with the addition level of dual-phased TiC_n-Al_3Ti_m particles. With 1 vol% dual-phased TiC_n-Al_3Ti_m particle addition, the $\sigma_{0.2}$ and σ_b were 53 MPa and 124 MPa, significantly improved by 43.2% and 87.9%, respectively, relative to the 37 MPa and 66 MPa of the unreinforced Pure Al. It is clear that the 5 vol% (TiC_n-Al_3Ti_m)/Al hybrid composite

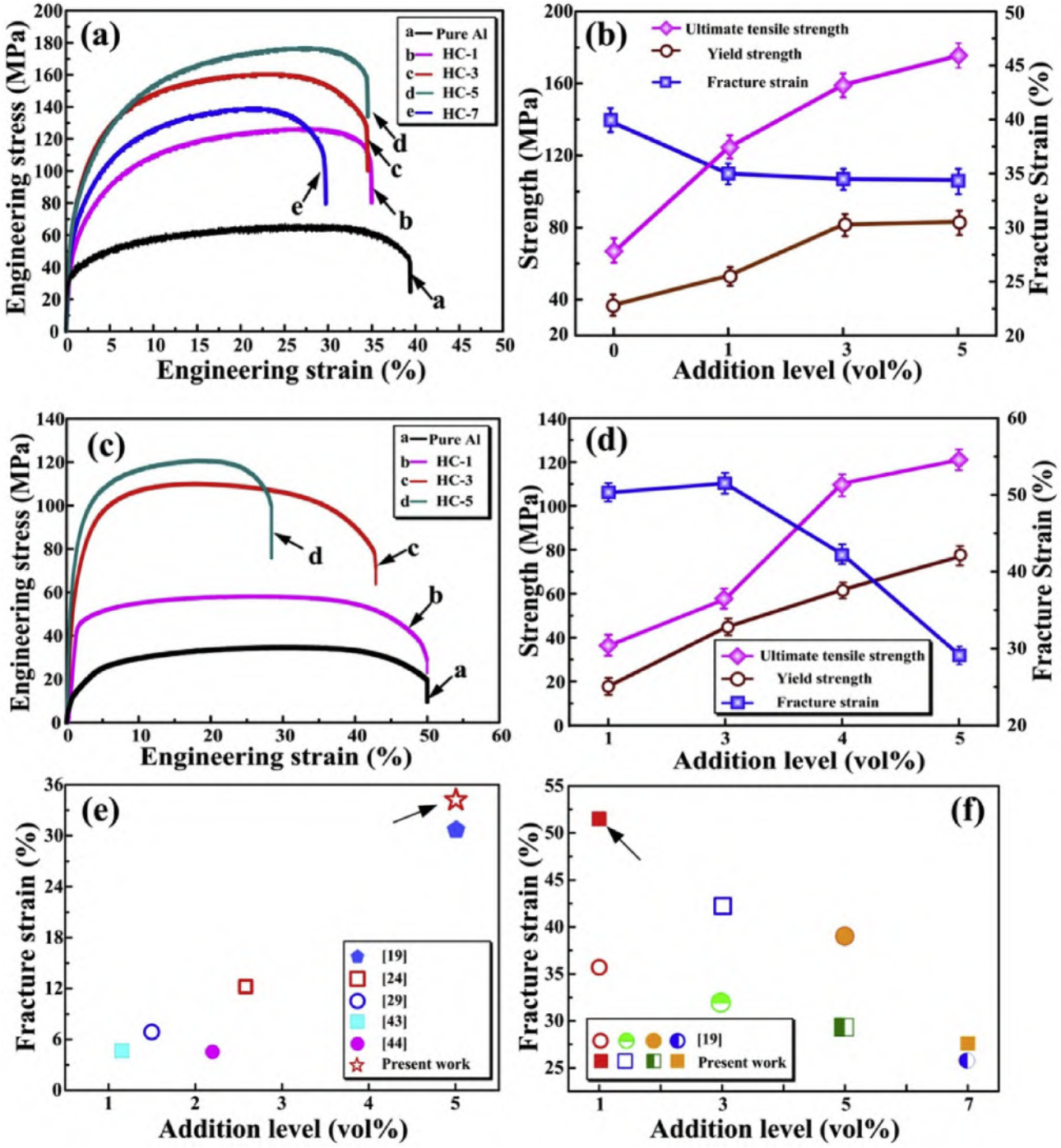

Fig. 9. (a) Tensile curves at 298 K of the prepared alloys with different addition levels of in situ dual-phased TiC_n-Al_3Ti_m particles and (b) the corresponding statistical analysis of the tensile properties; (c) Tensile curves at 453 K of the prepared alloys with different addition levels of in situ dual-phased TiC_n-Al_3Ti_m particles and (d) the corresponding statistical analysis of the tensile properties; comparison of the fracture strain as a function of the volume fraction of reinforced particles at (e) 298 K [19,24,29,43,44] and (f) 453 K [19].

Table 1
Tensile property values of the Pure Al and hybrid composites with various addition levels of in situ dual-phased TiC_n-Al_3Ti_m particles at 298 K and 453 K.

Sample	298 K	σ_b (MPa)	ε_f (%)	453 K	σ_b (MPa)	ε_f (%)
	$\sigma_{0.2}$ (MPa)			$\sigma_{0.2}$ (MPa)		
Pure Al	37 ± 0.3	66 ± 4.0	39.7 ± 3.3	18 ± 1.3	36 ± 2.6	50.3 ± 3.5
HC-1	53 ± 2.3	124 ± 3.0	35.0 ± 2.5	45 ± 2.0	58 ± 2.1	51.5 ± 1.8
HC-3	82 ± 3.0	159 ± 2.1	34.5 ± 2.3	62 ± 2.3	110 ± 3.6	42.3 ± 1.9
HC-5	83 ± 3.1	175 ± 2.9	34.4 ± 0.8	77 ± 3.2	121 ± 3.6	29.2 ± 2.5
HC-7	72 ± 3.6	139 ± 5.6	29.7 ± 4.3	50 ± 4.9	108 ± 5.8	27.6 ± 3.6

The uncertainty in the table is determined by ((Standard Deviation)/Average) × 100.

exhibited the best comprehensive properties, and the $\sigma_{0.2}$ and σ_b further increased to 83 MPa and 175 MPa, respectively, 124.3% and 165.2% higher than Pure Al. More importantly, distinguished from many pure Al composites reinforced by even lower addition levels, as shown in Fig. 9(e), desirable high fracture strains (ε_f) were retained for the fabricated hybrid composites reinforced by high addition levels of dual-phased TiC_n-Al_3Ti_m particles, breaking through the traditional strength-ductility trade-off of most composites. It is well understood that the ductility of composites is very significant for subsequent processing or engineering applications. Nevertheless, more addition of up to 7 vol% exerted an adverse impact on $\sigma_{0.2}$, σ_b and ε_f. This serious attenuation could be attributed to two reasons. On the one hand, as shown in Fig. 4(e), both the content and size of the tetragonally structured Al_3Ti phase increased at this addition level, particularly those at interdendritic regions or even across a whole α-Al grain. These particles will stimulate a severe stress concentration and then lead to early fracture. On the other hand, it is well known that the nanosized TiC particles are inclined to agglomerate into clusters, preferentially triggering crack initiation and propagation during tensile deformation.

3.3.2. Tensile properties at elevated temperature

To evaluate the heat resistance of the fabricated hybrid composites, tensile testing, of Pure Al, HC-1 and HC-5, at elevated temperature (at 453 K) was undertaken, as shown in Fig. 9(c and d) and Table 1. It is evident that the in situ dual-phased TiC_n-Al_3Ti_m particles still played a positive role in strengthening the pure Al matrix, and the substantial increments in strength were consistent with the tendency presented at ambient temperature. As observed, the unreinforced Pure Al exhibited lower $\sigma_{0.2}$ and σ_b (18 MPa and 36 MPa) than those of hybrid composites. The $\sigma_{0.2}$ and σ_b of the hybrid composite containing 1 vol% TiC_n-Al_3Ti_m particles were rapidly improved by 150% and 61.1%, respectively. More importantly, the fracture strain also showed a slight enhancement. With the increasing addition levels up to 5 vol%, the $\sigma_{0.2}$ and σ_b were further improved maximally to 77 MPa and 121 MPa, increases of 327.8% and 236.1%, respectively, whilst the ε_f was still at a relatively high level, up to 29.2%. Moreover, as shown in Fig. 9(f), the fabricated hybrid composites possess better fracture strain than their counterparts reinforced by nanosized SiC particles [19]. Comparatively, it is worthy to note that the fabricated TiC_n-Al_3Ti_m particles exhibited more efficient strengthening effects at an elevated temperature of 453 K than they did at ambient temperature.

3.3.3. Fracture behaviour

Typical fracture surfaces of the Pure Al, HC-1 and HC-5 alloys after tensile testing, at both 298 K and 453 K, are shown in Fig. 10. It can be observed that all the three alloys exhibited an obvious ductile fracture mode characterized by tear ridges and tiny dimples. Numerical dimples could be clearly seen in the low magnification micrographs Fig. 10(a–c) and (g-i), indicating that all the alloys experienced severe plastic deformation before failure. Obviously, the introduction of TiC_n-Al_3Ti_m particles made the dimples much more uniform, equiaxed, smaller and deeper than those of the unreinforced base alloy, which could be attributed to the remarkable grain refinement effects. These changes continued with the increasing addition level of hybrid particles, which commonly signified higher strength [45]. With the temperature increasing to 453 K, the dimples became larger and deeper when compared to those at 298 K. Moreover, it should be noted that few individual nanosized TiC particles, instead of Al_3Ti particles, were detected and visible at the core of the dimples, as revealed by the magnification micrographs Fig. 10 (f and l) of HC-5 alloy. It is reasonable that the micro-voids propagated preferentially at the interfaces between TiC/Al or Al_3Ti/Al due to their large difference in elastic modulus, followed by interface debonding or even fracture. While compared with those of the Al_3Ti/Al, the TiC/Al interfaces were more fragile and sensitive to the tensile loading due to the poor wettability between nanosized TiC and aluminum matrix.

3.4. Strengthening and toughening mechanisms of dual-phased (TiC_n-Al_3Ti_m)/Al hybrid composites

As mentioned above, excellent strengthening and toughening effects were simultaneously achieved at both ambient and elevated temperatures through the superiority of the in situ dual-phased and bimodal sized particles. Fig. 11 displays the schematic of the strengthening effects of TiC_n-Al_3Ti_m particles on the hybrid composites. It is generally accepted that the yield strength, at both ambient and elevated temperatures, is closely correlated with the interaction between the dislocation movements and reinforcement particles [19].

The strengthening mechanisms of these hybrid composites at ambient temperature could be ascribed to the synergistic effects of grain refinement and the well-dispersed particles, namely, grain-refinement strengthening, thermal-mismatch strengthening, Orowan strengthening and load-bearing strengthening mechanisms [46]. Given the low content of reinforcing particles with respect to the Al matrix, it is reasonable that the contributions of load-bearing strengthening are negligible.

As shown in Fig. 4(a–e), the microstructures of the hybrid composites were greatly refined by the added in situ dual-phased TiC_n-Al_3Ti_m particles. From the point of grain-refinement strengthening, the resultant more tortuous boundaries, as obstacles for dislocation passing, contribute to the improvement of yield strength. According to the classical Hall-Petch equation, the relationship between the grain size and yield strength could be expressed quantitatively as [47]:

$$\Delta\sigma_{HP} = k\left(d^{-1/2} - d_0^{-1/2}\right) \tag{2}$$

where k represents the Hall-Petch slope, and d and d_0 are the average grain sizes of the matrix and the hybrid composites.

Furthermore, large amounts of dislocations will be accumulated in the vicinity of the nanosized TiC particles and micron-sized Al_3Ti particles during solidification to accommodate the residual stress due to the incompatibility in the coefficient of thermal expansion (CTE) between the Al matrix and the nanosized TiC particles or micron-sized Al_3Ti particles. Thereby, the enhanced dislocation density will result in the notable increments of the yield strength, which could be quantitatively evaluated as below [47]:

$$\Delta\sigma_{CTE} = \eta G b \rho^{1/2} \tag{3}$$

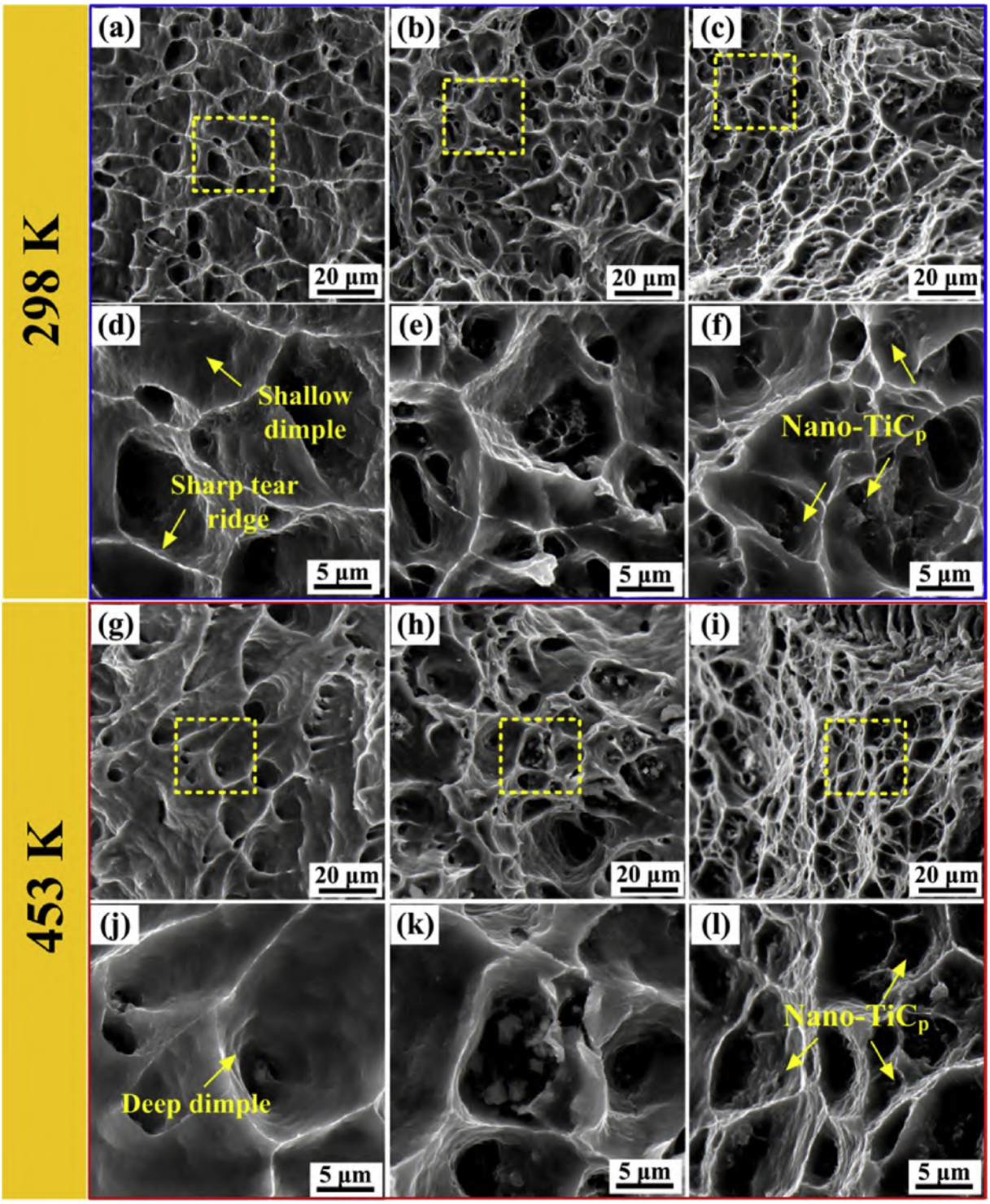

Fig. 10. Fracture surface micrographs of (a–c) low magnification and the corresponding (d–f) high magnification for the Pure Al, HC-1, HC-5, respectively, at 298 K. (g–i) Low magnification and the corresponding (j–l) high magnification fracture surface micrographs for the Pure Al, HC-1, HC-5, respectively, at 453 K.

$$\rho = 12\Delta\alpha\Delta T V_P/[bD(1 - V_P)] \quad (3a)$$

where η, G and b represent a constant of approximately 1.25, the shear modulus and Burgers vector of the matrix, respectively. V_P and D represent the volume fraction and average diameter of the reinforcements. $\Delta\alpha$ is the difference in CTE between the pure Al matrix and reinforcements. ΔT is the interval between the processing temperature and the mould temperature.

Additionally, Orowan strengthening induced by nanosized particles also contributes significantly to the yield strength increments of the hybrid composites. In our work, several nanosized TiC particles were engulfed into the growing dendrites during solidification, as seen in Figs. 6(a) and 8(b). Resultantly, the movement of

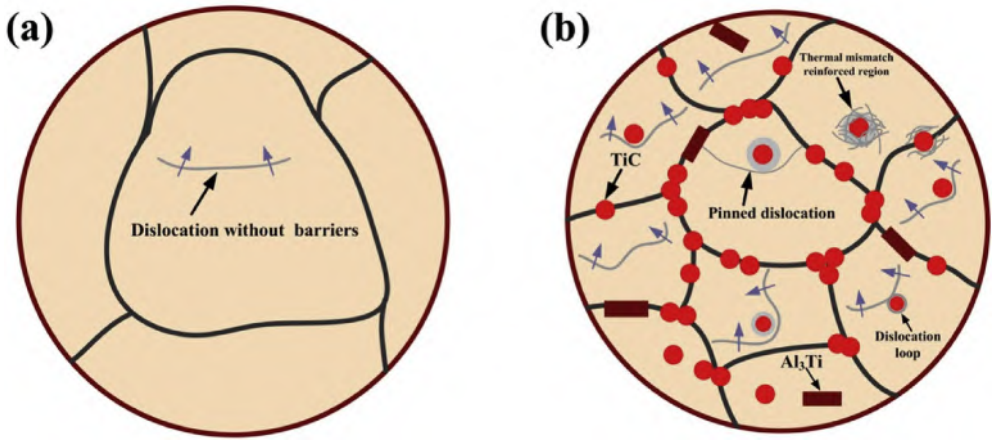

Fig. 11. Schematic diagrams showing the strengthening effects in (a) Pure Al and (b) (TiC_n-Al_3Ti_m)/Al hybrid composites.

dislocations will be strongly pinned and temporarily arrested by the closely spaced TiC particles, and thereafter, higher stress is required to activate these imprisoned dislocations. In this regard, the resistance of nanosized TiC particles to the dislocations also partially contributes to the enhancement in the yield strength, which could be calculated as below [47]:

$$\Delta\sigma_{Orwan} = 0.13Gb/\lambda \, In\frac{D}{2b} \tag{4}$$

where λ is the interparticle spacing of the incorporated TiC, expressed as:

$$\lambda = D\left[(2V_P)^{-1/3} - 1\right] \tag{4a}$$

In the present research, the comprehensive contribution of the in situ dual-phased TiC_n-Al_3Ti_m particles to the yield strength of the hybrid composites could be summarized as [47]:

$$\sigma_T = \sigma_0 + \Delta\sigma_{HP} + \left[(\Delta\sigma_{Orwan})^2 + (\Delta\sigma_{CTE})^2\right]^{1/2} \tag{5}$$

where σ_0 is the yield strength of pure Al matrix.

According to the equations (2)–(5) and the detailed reference parameters in Table 2, the individual contributions of the above strengthening mechanisms are calculated and summarized in Table 3. It can be concluded that the thermal-mismatch strengthening played the dominant role in determining the significant strengthening efficiency of the hybrid composites reinforced by in situ dual-phased TiC_n-Al_3Ti_m particles, followed by Orowan strengthening and grain-refinement strengthening. Furthermore,

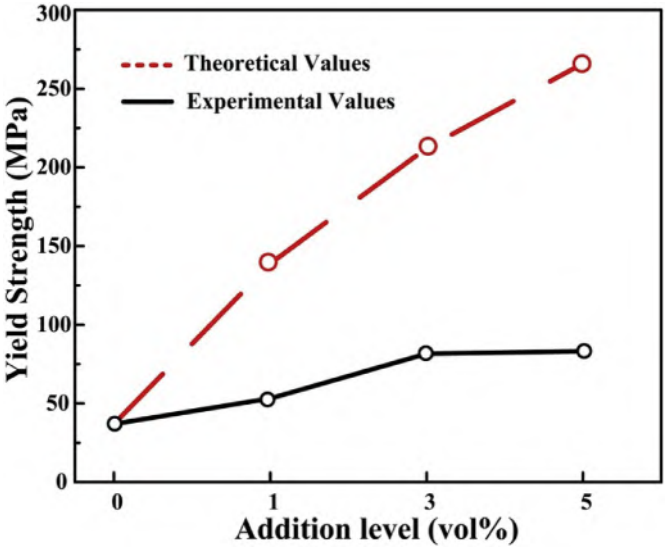

Fig. 12. Comparison analysis of the theoretical and experimental yield strength of the prepared hybrid composites.

as observed in Fig. 12, it is evident that the experimentally obtained yield strengths of the fabricated composites were far below the theoretical values. It is assumed that this consequence could be attributed to the lower strengthening efficiency of those large amounts of pushed nanosized TiC particles along the grain boundaries.

Table 2
The physical parameters used for theoretical calculations of the contributions of every strengthening mechanism to the yield strength of in situ dual-phased (TiC_n-Al_3Ti_m)/Al hybrid composites [13,19,44].

k (MPa μm$^{1/2}$)	G (GPa)	b (nm)	α_{Al} (10^{-6} K^{-1})	α_{TiC} (10^{-6} K^{-1})	α_{Al3Ti} (10^{-6} K^{-1})	ΔT (K)
74.0	26.2	0.286	23.6	8.6	13.0	560

Table 3
Theoretical calculation analysis of the contributions of every strengthening mechanism to the yield strength of in situ dual-phased (TiC_n-Al_3Ti_m)/Al hybrid composites.

Alloy	σ_0 (MPa)	$\Delta\sigma_{HP}$ (MPa)	$\Delta\sigma_{Orwan}$ (MPa)	$\Delta\sigma_{CTE}$ (MPa)	σ_T (MPa)	$\sigma_{0.2}$ (MPa)
HC-1	37.0	3.0	20.6	78.3	138.9	53.2
HC-3	37.0	3.6	35.1	136.6	212.3	81.6
HC-5	37.0	4.1	46.9	178.0	266.0	83.2

At elevated temperature, the more tortuous grain boundaries in the hybrid composites tend to become vulnerable places compared with their positive strengthening effect at ambient temperature [19]. The α-Al grains are inclined to viscous slip along the grain boundaries under an external tensile load. Moreover, more dislocation slip systems were initiated and became easier to slip, caused by the thermal activation with the rising temperature [48]. However, as indicated in Fig. 11(b), those nanosized TiC particles, pushed along the grain boundary regions, exerted "zener pinning" effect and served as stiff barriers or thermostable skeletons for the softening Al matrix to hinder the slipping behaviours of grain boundaries, which powerfully strengthened the matrix [11,49]. Additionally, dislocation slipping behaviors are also strongly pinned by the engulfed nanosized particles, resulting in great enhancement in yield strength at elevated temperature through Orowan strengthening mechanism. It is well understood that this strengthening effect will be improved continually as the addition level increases. Furthermore, the dislocation climbing behaviors may be thermally activated at elevated temperatures (>0.5 T_m, T_m is the absolute melt temperature of pure Al) [15,50]. Hence, it is assumed that the retarding effect of TiC_n-Al_3Ti_m particles to dislocation climbing, in the hybrid composites, also contributed to the prominent strength enhancement at elevated temperature in the present work.

With regard to the desirable fracture strains of the as-fabricated hybrid composites, it could be attributed to three aspects. First, the α-Al grains of the hybrid composites are significantly refined by the dual-phased TiC_n-Al_3Ti_m particles, thus, the paths for crack propagation are prolonged and delayed. Second, it is well known that the fracture strains of the composites are greatly sensitive to the size distribution and morphologies of the reinforcements. In our work, nanosized TiC particles with a spheroidal shape facilitate the synergistic deformation of the hybrid composites under external loading. Moreover, the content and size of brittle Al_3Ti intermetallic particles are properly controlled. Third, the clean and well-bonded interfaces are obtained between the matrix and the in situ particles, and the brittle interface reaction products or pores are avoided, which also greatly contribute to the fracture strain [19].

4. Conclusions

(1) Bimodal-sized and dual-phased TiC_n-Al_3Ti_m particles were in situ synthesized in an Al-Ti-C system via combustion synthesis method. Nanosized TiC particles were obtained with an average size of 80 nm and presented a spheroidal shape. Moreover, the micron-sized Al_3Ti particles were quantitatively controlled.

(2) The in situ dual-phased TiC_n-Al_3Ti_m particles exerted a prominent refinement effect on the α-Al dendrites. The finest average grain size was reduced by 74.1% in contrast with that of unreinforced Pure Al. During solidification, the recalescence phenomenon was suppressed, and the nucleation temperatures were shifted to higher temperatures in the presence of TiC_n-Al_3Ti_m particles, indicating that the in situ dual-phased TiC_n-Al_3Ti_m particles were efficient in promoting the nucleation of α-Al crystals. Specifically, grain refinement could be attributed to the heterogeneous nucleation of α-Al initiated by micron-sized Al_3Ti particles and powerfully inhibited growth of α-Al induced by nanosized TiC particles.

(3) At ambient temperature, the strengthening effects of the in situ dual-phased TiC_n-Al_3Ti_m were gradually improved with increasing addition levels. Compared with those of the base alloy, the highest yield strength and ultimate tensile strength of the hybrid composite were achieved with 5 vol% TiC_n-Al_3Ti_m particle addition, substantially improved by 124.3% and 165.2%. Note that an appropriate fracture strain was also retained and could reach up to 35%. The theoretical analysis indicated that thermal-mismatch and Orowan strengthening mechanisms play the dominant roles in the yield strength increment. Nevertheless, grain refinement greatly contributed to the desirable fracture strain.

(4) At elevated temperature (453 K), the hybrid composites also exhibited better thermal stability than that of the Pure Al. In the case of the 5 vol% addition level, the yield strength and ultimate tensile strength were increased up to 327.8% and 236.1%, respectively, whilst retaining a suitable ductility. It is worthy to note that the TiC_n-Al_3Ti_m particles exhibited more efficient strengthening effects at the elevated temperature (453 K) than they did at ambient temperature. The improved strength could be attributed to the pinning and retarding effects of the dual-phased TiC_n-Al_3Ti_m particles to the grain boundaries and dislocation movements.

Acknowledgements

This work is supported by the National Natural Science Foundation of China (NNSFC, No. 51571101 and No. 51771081), the Source Innovation Plan of Qingdao City, China (No. 18-2-2-1-jch), the Science and Technology Development Program of Jilin Province, China (20190302004GX).

References

[1] N. Muralidharan, K. Chockalingam, I. Dinaharan, K. Kalaiselvan, Microstructure and mechanical behavior of AA2024 aluminum matrix composites reinforced with in situ synthesized ZrB_2 particles, J. Alloys Compd. 735 (2018) 2167–2174.
[2] X. Ma, Y.F. Zhao, X.J. Zhao, J.F. Nie, H.W. Chen, X.F. Liu, Mechanisms on the outstanding high temperature plasticity of AlN_p/Al-0.4Cu composites induced by cryogenic treatment, J. Alloys Compd. 770 (2019) 755–764.
[3] Y.Y. Chen, Z.P. Hu, Y.F. Xu, J.Y. Wang, P. Schützendübe, Y. Huang, Y.C. Liu, Z.M. Wang, Microstructure evolution and interface structure of Al-40 wt% Si composites produced by high-energy ball milling, J. Mater. Process. Technol. 35 (2019) 512–519.
[4] B. Dang, X. Zhang, Y.Z. Chen, C.X. Chen, H.T. Wang, F. Liu, Breaking through the strength-ductility trade-off dilemma in an Al-Si-based casting alloy, Sci. Rep. 6 (2016) 30874.
[5] Q.F. Xu, X. Ma, K.Q. Hu, T. Gao, X.F. Liu, A novel (AlN + Si_3N_4)/Al composite with well-balanced strength and ductility, Mater. Sci. Eng. A 726 (2018) 113–119.
[6] C.J. Hsu, C.Y. Chang, P.W. Kao, N.J. Ho, C.P. Chang, Al-Al_3Ti nanocomposites produced in situ by friction stir processing, Acta Mater. 54 (2006) 5241–5249.
[7] S.L. Lü, P. Xiao, D. Yuan, K. Hu, S.S. Wu, Preparation of Al matrix nanocomposites by diluting the composite granules containing nano-SiC_p under ultrasonic vibration, J. Mater. Sci. Technol. 34 (2018) 1609–1617.
[8] Q. Gao, S.S. Wu, S.L. Lü, X.C. Xiong, R. Du, P. An, Improvement of particles distribution of in-situ 5 vol% TiB_2 particulates reinforced Al-4.5Cu alloy matrix composites with ultrasonic vibration treatment, J. Alloys Compd. 692 (2017) 1–9.
[9] L. Zhou, C. Cui, Q.Z. Wang, C. Li, B.L. Xiao, Z.Y. Ma, Constitutive equation and model validation for a 31 vol.% B_4C_p/6061Al composite during hot compression, J. Mater. Sci. Technol. 34 (2018) 1730–1738.
[10] M.P. Reddy, F. Ubaid, R.A. Shakoor, G. Parande, V. Manakari, A.M.A. Mohamed, M. Gupta, Effect of reinforcement concentration on the properties of hot extruded Al-Al_2O_3 composites synthesized through microwave sintering process, Mater. Sci. Eng. A 696 (2017) 60–69.
[11] H.B. Yang, T. Gao, Y.Y. Wu, H.N. Zhang, J.F. Nie, X.F. Liu, Microstructure and mechanical properties at both room and high temperature of in-situ TiC reinforced Al-4.5Cu matrix nanocomposite, J. Alloys Compd. 767 (2018) 606–616.
[12] J. Qin, G. Chen, X.H. Ji, X.G. Song, N. Hu, F. Han, Z.M. Du, Effect of reaction temperature on the microstructures and mechanical properties of high-intensity ultrasonic assisted in-situ Al_3Ti/2024 Al composites, J. Alloys Compd. 666 (2016) 58–64.
[13] Z.W. Liu, N. Cheng, Q.L. Zheng, J.H. Wu, Q.Y. Han, Z.F. Huang, J.D. Xing, Y.F. Li, Y.M. Gao, Processing and tensile properties of A356 composites containing in situ small-sized Al_3Ti particulates, Mater. Sci. Eng. A 710 (2018) 392–399.
[14] B. Yang, G.S. Gan, L. Yang, M. Sun, H.B. Zhang, Z.Z. Fang, Microstructural characterization and wear behavior of in situ TiC/7075 composites synthesized by displacement reactions and spray forming, Mater. Sci. Eng. A 528 (2011) 5649–5655.

[15] W.S. Tian, Q.L. Zhao, Q.Q. Zhang, F. Qiu, Q.C. Jiang, Simultaneously increasing the high-temperature tensile strength and ductility of nano-sized TiC_p reinforced Al-Cu matrix composites, Mater. Sci. Eng. A 717 (2018) 105–112.

[16] N. Samer, J. Andrieux, B. Gardiola, N. Karnatak, O. Martin, H. Kurita, L. Chaffron, S. Gourdet, S. Lay, O. Dezellus, Microstructure and mechanical properties of an Al-TiC metal matrix composite obtained by reactive synthesis, Composites Part A 72 (2015) 50–57.

[17] M.X. Zhang, P.M. Kelly, M.A. Easton, J.A. Taylor, Crystallographic study of grain refinement in aluminum alloys using the edge-to-edge matching model, Acta Mater. 53 (2005) 1427–1438.

[18] Z. Fan, Y. Wang, Y. Zhang, T. Qin, X.R. Zhou, G.E. Thompson, T. Pennycook, T. Hashimoto, Grain refining mechanism in the Al/Al-Ti-B system, Acta Mater. 84 (2015) 292–304.

[19] Q. Li, F. Qiu, B.X. Dong, R. Geng, M.M. Lv, Q.L. Zhao, Q.C. Jiang, Fabrication, microstructure refinement and strengthening mechanisms of nanosized SiC_P/Al composites assisted ultrasonic vibration, Mater. Sci. Eng. A 735 (2018) 310–317.

[20] W.S. Tian, Q.L. Zhao, Q.Q. Zhang, F. Qiu, Q.C. Jiang, Enhanced strength and ductility at room and elevated temperatures of Al-Cu alloy matrix composites reinforced with bimodal-sized TiC_p compared with monomodal-sized TiC_p, Mater. Sci. Eng. A 724 (2018) 368–375.

[21] L.J. Zhang, F. Qiu, J.G. Wang, H.Y. Wang, Q.C. Jiang, Microstructures and mechanical properties of the Al2014 composites reinforced with bimodal sized SiC particles, Mater. Sci. Eng. A 637 (2015) 70–74.

[22] M.J. Shen, X.J. Wang, M.F. Zhang, M.Y. Zheng, K. Wu, Significantly improved strength and ductility in bimodal-size grained microstructural magnesium matrix composites reinforced by bimodal sized SiC_p over traditional magnesium matrix composites, Compos. Sci. Technol. 118 (2015) 85–93.

[23] M.O. Bodunrina, K.K. Alaneme, L.H. Chown, Aluminium matrix hybrid composites: a review of reinforcement philosophies; mechanical, corrosion and tribological characteristics, J. Mater. Res. Technol. 4 (2015) 434–445.

[24] H.F. Dehkordi, M.R. Toroghinejad, K. Raeissi, Fabrication of Al/Al_2O_3/TiC hybrid composite by anodizing and accumulative roll bonding processes and investigation of its microstructure and mechanical properties, Mater. Sci. Eng. A 585 (2013) 460–467.

[25] E.A.M. Shalaby, A.Y. Churyumov, A.N. Solonin, A. Lotfy, Preparation and characterization of hybrid A359/(SiC_p+Si_3N_4) composites synthesized by stir/squeeze casting techniques, Mater. Sci. Eng. A 674 (2016) 18–24.

[26] B.K. Show, D.K. Mondal, K. Biswas, J. Maity, Development of a novel 6351 Al-(Al_4SiC_4+SiC) hybrid composite with enhanced mechanical properties, Mater. Sci. Eng. A 579 (2013) 136–149.

[27] Q.Y. Hu, H.D. Zhao, J.L. Ge, Microstructure and mechanical properties of (B_4C+Al_3Ti)/Al hybrid composites fabricated by a two-step stir casting process, Mater. Sci. Eng. A 650 (2016) 478–482.

[28] X.R. Chen, D.F. Fu, J. Teng, H. Zhang, Hot deformation behavior and mechanism of hybrid aluminum matrix composites reinforced with micro-SiC and nano-TiB2, J. Alloys Compd. 753 (2018) 566–575.

[29] M.P. Reddy, V. Manakari, G. Parande, F. Ubaid, R.A. Shakoor, A.M.A. Mohamed, M. Gupta, Enhancing compressive, tensile, thermal and damping response of pure Al using BN nanoparticles, J. Alloys Compd. 762 (2018) 398–408.

[30] X.F. Du, T. Gao, G.L. Liu, X.F. Liu, In situ synthesizing SiC particles and its strengthening effect on an Al-Si-Cu-Ni-Mg piston alloy, J. Alloys Compd. 695 (2017) 1–8.

[31] C.C. Yang, Z.W. Liu, Q.L. Zheng, Y.L. Cao, X.H. Dai, L. Sun, J.R. Zhao, J.D. Xing, Q.Y. Han, Ultrasound assisted in-situ casting technique for synthesizing small-sized blocky Al_3Ti particles reinforced A356 matrix composites with improved mechanical properties, J. Alloys Compd. 747 (2018) 580–590.

[32] C. Li, G. Sha, J.H. Xia, Y.C. Liu, S.P. Ringer, Si-induced precipitation modification and related age-hardening response of an Al-4Mg-1Cu-0.5Si alloy, Mater. Chem. Phys. 193 (2017) 421–426.

[33] Y.F. Zhao, X. Ma, X.J. Zhao, H.W. Chen, X.F. Liu, Enhanced aging kinetic of Al_3BC/6061 Al composites and its micro-mechanism, J. Alloys Compd. 726 (2017) 1053–1061.

[34] H. Yu, N. Wang, R.G. Guan, D. Tie, Z. Li, Y.N. An, Y. Zhang, Evolution of secondary phase particles during deformation of Al-5Ti-1B master alloy and their effect on α-Al grain refinement, J. Mater. Sci. Technol. 34 (2018) 2297–2306.

[35] R. Tao, Y.T. Zhao, X.Z. Kai, Y. Wang, W. Qian, Y.G. Yang, M. Wang, W.T. Xu, The effects of Er addition on the microstructure and properties of an in situ nano ZrB_2-reinforced A356.2 composite, J. Alloys Compd. (2018) 200–209.

[36] E. Ghasali, R. Yazdani-rad, K. Asadian, T. Ebadzadeh, Production of Al-SiC-TiC hybrid composites using pure and 1056 aluminum powders prepared through microwave and conventional heating methods, J. Alloys Compd. 690 (2017) 512–518.

[37] Q. Tang, J.H. Zhao, T. Wang, J. Chen, K. He, The effects of neodymium addition on the intermetallic microstructure and mechanical properties of Al-7Si-0.3Mg-0.3Fe alloys, J. Alloys Compd. 741 (2018) 161–173.

[38] H.B. Yang, Z. Qian, G.J. Zhang, J.F. Nie, X.F. Liu, The grain refinement performance of B-doped TiC on Zr-containing Al alloys, J. Alloys Compd. 731 (2018) 774–783.

[39] I. Maxwell, A. Hellawell, A simple model for grain refinement during solidification, Acta Metall. 23 (2) (1975) 229–237.

[40] D. Qiu, M.X. Zhang, The nucleation crystallography and wettability of Mg grains on active Al_2Y inoculants in an Mg-10 wt% Y alloy, J. Alloys Compd. 586 (2014) 39–44.

[41] H.T. Li, M. Xia, Ph. Jarry, G.M. Scamans, Z. Fan, Grain refinement in a AlZnMgCuTi alloy by intensive melt shearing: a multi-step nucleation mechanism, J. Cryst. Growth 314 (2011) 285–292.

[42] Z.Y. Zhang, G. Chen, S.L. Zhang, Y.T. Zhao, R. Yang, M.P. Liu, Enhanced strength and ductility in ZrB_2/2024Al nanocomposite with a quasi-network architecture, J. Alloys Compd. 778 (2019) 833–838.

[43] M. Zabihi, M.R. Toroghinejad, A. Shafyei, Application of powder metallurgy and hot rolling processes for manufacturing aluminum/alumina composite strips, Mater. Sci. Eng. A 560 (2013) 567–574.

[44] W.J. Kim, Y.J. Yu, The effect of the addition of multiwalled carbon nanotubes on the uniform distribution of TiC nanoparticles in aluminum nanocomposites, Scr. Mater. 72–73 (2014) 25–28.

[45] H.B. Yang, T. Gao, H.N. Zhang, J.F. Nie, X.F. Liu, Enhanced age-hardening behavior in Al-Cu alloys induced by in-situ synthesized TiC nanoparticles, J. Mater. Sci. Technol. 35 (2019) 374–382.

[46] F. Chen, Z.N. Chen, F. Mao, T.M. Wang, Z.Q. Cao, TiB_2 reinforced aluminum based in situ composites fabricated by stir casting, Mater. Sci. Eng. A 625 (2015) 357–368.

[47] N. Srivastava, G.P. Chaudhari, Microstructural evolution and mechanical behavior of ultrasonically synthesized Al6061-nano alumina composites, Mater. Sci. Eng. A 724 (2018) 199–207.

[48] K.Q. Hu, Q.F. Xu, X. Ma, Q.Q. Sun, T. Gao, X.F. Liu, A novel heat-resistant Al–Si–Cu–Ni–Mg base material synergistically strengthened by Ni-rich intermetallics and nano-AlN_p microskeletons, J. Mater. Sci. Technol. 35 (2019) 306–312.

[49] J.W. Geng, T.R. Hong, Y.W. Shen, G. Liu, C.J. Xia, D. Chen, M.L. Wang, H.W. Wang, Microstructural stability of in-situ TiB_2/Al composite during solution treatment, Mater. Char. 124 (2017) 50–57.

[50] J. Qin, Z. Zhang, X.G. Chen, Mechanical properties and strengthening mechanisms of Al-15 Pct B_4C composites with Sc and Zr at elevated temperatures, Metall. Mater. Trans. A 47 (2016) 4694–4708.